Published in final edited form as:
Chem Eng Sci. 2010 October 15; 65(20): 5471–5481. doi:10.1016/j.ces.2010.07.011.

Design of Aerosol Particle Coating: Thickness, Texture and Efficiency

B. Buesser and **S.E. Pratsinis***
Particle Technology Laboratory, Institute of Process Engineering, Department of Mechanical and Process Engineering, ETH Zurich, 8092 Zürich, Switzerland

Abstract

Core-shell particles preserve the performance (e.g. magnetic, plasmonic or opacifying) of a core material while modifying its surface with a shell that facilitates (e.g. by blocking its reactivity) their incorporation into a host liquid or polymer matrix. Here coating of titania (core) aerosol particles with thin silica shells (films or layers) is investigated at non-isothermal conditions by a trimodal aerosol dynamics model, accounting for SiO_2 generation by gas phase and surface oxidation of hexamethyldisiloxane (HMDSO) vapor, coagulation and sintering. After TiO_2 particles have reached their final primary particle size (e.g. upon completion of sintering during their flame synthesis), coating starts by uniformly mixing them with HMDSO vapor that is oxidized either in the gas phase or on the particles' surface resulting in SiO_2 aerosols or deposits, respectively. Sintering of SiO_2 deposited onto the core TiO_2 particles takes place transforming rough into smooth coating shells depending on process conditions. The core-shell characteristics (thickness, texture and efficiency) are calculated for two limiting cases of coating shells: perfectly smooth (e.g. hermetic) and fractal-like. At constant TiO_2 core particle production rate, the influence of coating weight fraction, surface oxidation and core particle size on coating shell characteristics is investigated and compared to pertinent experimental data through coating diagrams. With an optimal temperature profile for complete precursor conversion, the TiO_2 aerosol and SiO_2-precursor (HMDSO) vapor concentrations have the strongest influence on product coating shell characteristics.

Keywords

particle formation; hermetic layering; population balance; condensation; nanoparticle encapsulation; powder technology

1. Introduction

Particles are frequently coated to facilitate their processing (e.g. reduce agglomeration) and enhance their performance by making them compatible with solid or liquid host matrices (Egerton, 1998). With such core-shell particles, one conserves the properties of the core material (e.g. dielectric, magnetic, plasmonic, scattering or opacifying functions) while modifying its surface with a shell material. For example, pigmentary rutile TiO_2 particles are made by the "chloride" or "sulfate" process (Mezey, 1966). They are coated with silica, alumina and other oxides by wet impregnation processes to prevent the photocatalytic activity of TiO_2 with the host solvent, die or polymer (Clark, 1975) and reduce its agglomeration in paints (Egerton, 1998).

*Corresponding author: +41-44-632-3180; fax: -1595; pratsinis@ptl.mavt.ethz.ch.

Europe PMC Funders Author Manuscripts

Though wet phase coating of particles has been practiced for long and even for large scale manufacture of commodities, it is a demanding and costly process (Fisher and Egerton, 2001). An alternative route is to coat particles by gas phase processes that do not involve liquid by-products, offer easier particle collection and can reduce the multiple steps of wet processes (Pratsinis and Mastrangelo, 1989). Despite its advantages, coating of particles in the gas phase is challenging, as particle growth is much faster than in liquids. As a result, it is quite difficult to control and develop a scalable gas phase coating process. So, even commercial particles made by aerosol routes (e.g. TiO_2 made by the "chloride" process) are always coated by wet processes.

Despite this industrial "reality", significant effort has been made in understanding the fundamentals of aerosol particle coating in academic laboratories and developing such processes industrially (Subramanian *et al.*, 2006). Hung and Katz (1992) investigated the formation of mixed TiO_2-SiO_2 powders in a counter-flow diffusion burner and identified conditions for synthesis of such core-shell particles by varying the inlet Si/Ti from 0.15 to 3. Akhtar *et al.* (1992) made TiO_2-SiO_2 particles by co-oxidation of their chloride precursors in a hot-wall reactor and found silica films on TiO_2 by X-ray photoelectron spectroscopy at inlet Si/Ti = 0.04 - 0.20. Fotou *et al.* (1994) made and simulated flame-coating of suspended fibers with smooth or rough layers by controlling the sintering rate of flame-made silica coating particles. Powell *et al.* (1997a,b) deposited silica or alumina coatings on TiO_2 particles made in a hot-wall reactor at inlet SiO_2/TiO_2 = 0.007 - 0.18. Increasing the flow rate of the coating precursor ($SiCl_4$ or $AlCl_3$) led to rougher coatings by formation of separate silica or alumina particles. Improving the mixing of the coating precursor with the core particles led to smoother coating shells. A moment model was developed for this process at isothermal conditions by Jain *et al.* (1997) that was in qualitative agreement with Powell *et al.* (1997a). Ehrman *et al.* (1998) made SiO_2/TiO_2 particles including coated ones in a premixed flame reactor at inlet Si/Ti = 1. Teleki *et al.* (2005) observed smooth SiO_2 coatings on TiO_2 particles by rapid quenching of the flame with a critical flow nozzle (Wegner *et al.*, 2002). Rough and smooth coating shells were made at inlet Si/Ti = 0.33, otherwise segregated ones (Janus particles) were formed. King *et al.* (2008) have used atomic layer deposition to smoothly coat TiO_2 particles with SiO_2 layer-by-layer without increasing their aggregation in a fluidized bed. Sheen *et al.* (2009) made coated composite particles in a sliding co-flow diffusion flame at inlet Si/Ti = 4 - 57. Recently, Teleki *et al.* (2008) hermetically coated flame-made TiO_2 particles with nanothin SiO_2 (mole Si/Ti = 0.066 - 0.4) shells by injecting the SiO_2 precursor vapor into an enclosed flame reactor at a location where TiO_2 primary particle growth had been completed. The coating quality was determined by Raman, FT-IR, microscopy and photocatalysis of isopropanol in suspensions of these particles. Teleki *et al.* (2009a) showed also that improving the mixing between core aerosol and coating precursor vapor increases the fraction of coated core particles and the quality of coating, experimentally and by computational fluid dynamics.

Today, there is a reasonable understanding of what is needed to coat particles. For example, minimal coating thickness and high efficiency are required in coating TiO_2 or Fe_2O_3 particles to minimize the costs of coating material or maximize the bulk properties of the core particle like magnetization performance (Teleki *et al.*, 2009b). Smooth coatings give consistent optical performance while rough ones facilitate minimization of agglomeration (Egerton, 1998). Furthermore there is a reasonable understanding on how to control coating of aerosol-made particles in various laboratory scale flame, hot-wall or fluidized-bed aerosol reactors.

Here, emphasis is placed on the quantitative understanding of aerosol coating processes. Gas phase synthesis of nanothin coating shells on aerosol core primary particles is investigated theoretically accounting for monodisperse core (Kruis *et al.*, 1993) and bimodal coating

particle dynamics (Jeong and Choi, 2005) by coagulation, sintering and surface growth. Emphasis is placed on understanding the effect of aerosol process parameters and formation pathways, gas phase or surface reaction, on the efficiency of the process, texture of the coating shells (smooth or rough) and the equivalent thickness of the coating shell. The results of the simulations are compared with experimental data.

2. Theory

Figure 1 shows a schematic of the coating process (left hand side) and the evolution of the trimodal particle size distribution (right hand side). Core aerosol particles (e.g. TiO_2, white) that no longer sinter enter the coating unit with number concentration N_c well-mixed with coating precursor vapor (e.g. HMDSO, black dots) of concentration C. Coating monomers (e.g. SiO_2, blue dots) with concentration N_1 are generated by precursor oxidation (Ulrich, 1971) and coagulate either with core particles creating immediately smooth shells of volume concentration V_s or among themselves forming fractal-like or spherical coating particles of concentration N_2 with surface area and volume concentrations A_2 and V_2, respectively. These coating particles result in rough shells of area and volume concentration A_r and V_r, respectively, by coagulation with core particles. Rough shells are smoothed out by sintering, depending on their (primary) particle diameter, d_{pr}, and temperature. Oxidation of coating vapor (e.g. HMSDO) may take place also on the surface of core or coating particles leading to smooth shells or bigger coating particles, respectively. Core particles coagulate to form agglomerates but not aggregates as their coating takes place when their sintering has ended (Tsantilis and Pratsinis, 2004). So their number concentration N_c changes but the total number of core primary particles is constant.

During HMDSO vapor oxidation in the gas phase, coating (SiO_2) monomers are formed that grow into large coating particles by coagulation or deposit onto core particles forming smooth shells (Fig. 1a). Also HMDSO can decompose onto the particles forming SiO_2 by surface reaction. As the HMDSO oxidation ceases, coating monomers are depleted while coating particles start to deposit onto the core particles to form rough shells and a typical bimodal coating monomer/particle distribution develops (Fig. 1b). As coating monomers disappear, coating aggregates and agglomerates form a unimodal distribution and deposit onto the core particles while rough shells are smoothed out by sintering (Fig. 1c).

2.1 Oxidation of coating precursor

The coating precursor vapor (e.g. HMDSO) can react with oxygen either in the gas phase, generating coating monomers or on particle surfaces, leading to surface growth. So the overall oxidation rate of coating precursor vapor is:

$$\frac{dC}{dt} = -kC - \frac{C}{Q}\frac{dQ}{dt} = -\left(k_g + k_s\right)C - \frac{C}{Q}\frac{dQ}{dt} \quad (1)$$

The first right hand side (RHS) term accounts for the overall (gas phase and surface) oxidation of HMDSO:

$$C_6H_{18}OSi_2 + 12\ O_2 \rightarrow 2\ SiO_2 + 6\ CO_2 + 9H_2O$$

with $k = 4\times10^{17}\exp(-3.7\times10^5/(8.314\times T))\ s^{-1}$ (Ehrman *et al.*, 1998). The second RHS term accounts for the change in gas volume and composition by cooling and reaction. The gas flow rate, Q, is calculated by ideal gas law accounting for the concentration of each gaseous species including the reaction above and changes in temperature (Heine and Pratsinis, 2006).

The overall surface oxidation rate of HMDSO is not known., but its impact on coating can be estimated here considering that it encompasses two steps: a) transport of HMDSO molecules to the particle surface and b) their oxidation there. The rate of HMDSO transport to coating and core particles is determined by their respective collision frequencies, $\beta_{p,2}$ and $\beta_{p,c}$. When there is no information about the second step, the oxidation rate of the colliding molecules on the particle surface (e.g. surface oxidation of HMDSO), the overall surface oxidation rate constant, k_s, for transport and reaction can be written as:

$$k_s=\alpha_2\beta_{p,2}N_2+\alpha_c\beta_{p,c}N_c \quad (2)$$

where $\beta_{p,2}N_2$ and $\beta_{p,c}N_c$ describe the rate of transport of HMDSO molecules to the surface of coating and core particles, respectively. The α_2 and α_c describe the fraction of arriving HMDSO molecules that are oxidized on the particle surface (Friedlander, 2000), also called efficiency of collisions. Assuming for simplicity $\alpha = \alpha_2 = \alpha_c$, two limiting cases then are distinguished: for instantaneous surface reaction $\alpha = 1$ and no surface reaction $\alpha = 0$. Molecules that have not been oxidized on the particle surface (e.g. the fraction 1-α) return into the gas phase immediately after collision.

For a finite overall surface reaction rate (α nonzero) with reaction order equal to that of the overall gas phase reaction (e.g. $TiCl_4$ (Pratsinis and Spicer, 1998)) the gas phase oxidation rate constant, k_g, is defined for an overall surface oxidation rate smaller than the overall oxidation rate ($k_s < k$) as the difference between the two oxidation rate constants (Pratsinis and Spicer, 1998; Tsantilis *et al.*, 2002):

$$k_g=k-k_s \quad (3a)$$

$$\alpha=\alpha_{max} \quad (3b)$$

where α_{max} is the maximum value which usually has to be determined experimentally (Friedlander, 2000). When the aerosol surface area increases so much that the estimated overall surface oxidation rate becomes higher than the overall oxidation rate ($k_s > k$), surface reaction dominates and gas phase reaction stops. In the model the gas phase oxidation rate constant and the fraction of successful collisions are defined then as (Tsantilis *et al.*, 2002):

$$k_g=0 \quad (4a)$$

$$\alpha=\frac{k}{\left(\beta_{p,2}N_2+\beta_{p,c}N_c\right)} \quad (4b)$$

So the surface oxidation rate of the coating precursor vapor does not exceed the experimentally determined k and the gas-phase generation of coating monomers stops (k_g = 0) while coating precursor vapor is oxidized only on particle surfaces. Here calculations are carried out for the two limiting cases $\alpha_{max} = 1$ and $\alpha_{max} = 0$.

2.2 Coating particle dynamics

The evolution of coating monomers (index *1*) and particles (index *2*) is described with a bimodal model (Jeong and Choi, 2005) extended for coagulation with core particles (index *c*) but without surface growth on monomers as here the coating precursor (HMDSO) generates two monomers per molecule ($n_m = 2$). The coating monomers represent the smallest possible coating particle (Ulrich, 1971) corresponding to SiO_2 molecules with a diameter of 0.4 nm (Xiong and Pratsinis, 1991).

The rate of change of the coating monomer number concentration, N_1, is:

$$\frac{dN_1}{dt} = n_m k_g C - \frac{1}{2}\beta_1 N_1^2 \frac{r}{r-1} - \beta_{1,2} N_1 N_2 - \beta_{1,c} N_1 N_c - \frac{N_1}{Q}\frac{dQ}{dt} \quad (5)$$

where $n_m = 2$ for HMDSO. The collision frequencies, β, are calculated with the Fuchs interpolation function (Kruis *et al.*, 1993). The size ratio $r = v_2/v_1$ weighs monomer-monomer collisions and preserves the particle number and volume concentration (Jeong and Choi, 2003). The first RHS term describes formation of coating monomers by gas phase oxidation. The second and third RHS terms account for the loss of coating monomers by coagulation with monomers and coating particles, respectively. The fourth accounts for the loss of coating monomers by coagulation with core particles (forming smooth coating shells) and the fifth for the changing gas flow rate.

The rate of change of coating particle number concentration, N_2, is:

$$\frac{dN_2}{dt} = \frac{1}{2}\beta_{1,1} N_1^2 \frac{1}{r-1} - \frac{1}{2}\beta_{2,2} N_2^2 - \beta_{2,c} N_2 N_c - \frac{N_2}{Q}\frac{dQ}{dt} \quad (6)$$

The first RHS term describes the gain by coagulation of coating monomers, the second and third RHS terms account for the loss of coating particles by coagulation among themselves and with core particles (forming rough coating shells). The fourth RHS term accounts for the changing gas flow rate.

The rate of change of surface area concentration of coating particles, A_2, is similar to equation 6 and defined as:

$$\frac{dA_2}{dt} = \frac{1}{2}\beta_{1,1} N_1^2 a_1 \frac{r}{r-1} + \beta_{1,2} N_1 N_2 a_1 - \beta_{2,c} N_2 N_c a_2 - \frac{A_2 - N_2 a_{2f}}{\tau\left(d_{p2}\right)} + \frac{4}{d_{p2}}\alpha\beta_{p,2} C N_2 n_m v_1 - \frac{A_2}{Q}\frac{dQ}{dt} \quad (7)$$

The fourth RHS term describes the loss of A_2 by sintering of coating aggregates (Friedlander and Wu, 1994; Koch and Friedlander, 1990) and the fifth RHS term the gain by surface oxidation of coating precursor vapor (Jeong and Choi, 2005). The sintering time for SiO_2 has been calculated with the equation of Tsantilis *et. al* (2001) with $d_{p,min} = 1$ nm. Similarly, the rate of change of volume concentration of coating particles, V_2, is:

$$\frac{dV_2}{dt} = \frac{1}{2}\beta_{1,1} N_1^2 v_1 \frac{r}{r-1} + \beta_{1,2} N_1 N_2 v_1 + \alpha\beta_{p,2} C N_2 n_m v_1 - \beta_{2,c} N_2 N_c v_2 - \frac{V_2}{Q}\frac{dQ}{dt} \quad (8)$$

The collision diameter of coating particles for the calculation of β (Kruis *et al.*, 1993) is defined as (Heine and Pratsinis, 2006):

$$d_2 = d_{p2} n_{p2}^{\frac{1}{D_f}} = \frac{6V_2}{A_2}\left(\frac{A_2^3}{36\pi N_2 V_2^2}\right)^{\frac{1}{D_f}} \quad (9)$$

The coating particles grow as aggregates or agglomerates with constant fractal dimension $D_f = 1.8$ (Schaefer and Hurd, 1990).

2.3 Core particle dynamics

Coating of core particles is optimal when core primary particle growth (and their sintering) has stopped (Teleki *et al.*, 2008). As a result, during coating the initial core primary particle diameter, d_{pc}, and the total number of core primary particles, $N_c n_{pc}$, remains constant. So the evolution of the number concentration of core agglomerate particles, N_c, can be described by a monodisperse coagulation model:

$$\frac{dN_c}{dt} = -\frac{1}{2}\beta_{c,c}N_c^2 - \frac{N_c}{Q}\frac{dQ}{dt} \quad (10)$$

where the coagulation rate of core agglomerates is given by Kruis *et al.* (1993) with the core collision diameter from section 2.3.2 accounting for the coating shell.

2.3.1 Coating of core particles—The coating shells on the core primary particles are distinguished into rough and smooth and described by their surface area and volume concentrations. So, the rate of change of rough coating shell surface area concentration, A_r, is:

$$\frac{dA_r}{dt} = \beta_{2,c}N_2N_c a_2 - \frac{A_r}{\tau\left(d_{pr}\right)} - \frac{A_r}{Q}\frac{dQ}{dt} \quad (11)$$

where d_{pr} is the primary particle diameter of the coating aggregates making up the rough coating shells: $d_{pr} = 6V_r/A_r$ (Fotou *et al.*, 1994). The first RHS term describes the surface area increase by coagulation of coating and core particles, the second RHS term accounts for the loss A_r by sintering of rough into smooth coating shell lamellae that have negligible surface area (Appendix). Similarly, the rate of change of rough coating shell volume concentration, V_r, is given by:

$$\frac{dV_r}{dt} = \beta_{2,c}N_2N_c v_2 - \frac{V_r}{\tau\left(d_{pr}\right)} - \frac{V_r}{Q}\frac{dQ}{dt} \quad (12)$$

The rate of change of smooth coating shell volume concentration, V_s, is given by:

$$\frac{dV_s}{dt} = \beta_{1,c}N_1N_c v_1 + \frac{V_r}{\tau\left(d_{pr}\right)} + \alpha\beta_{p,c}CN_c n_m v_1 - \frac{V_s}{Q}\frac{dQ}{dt} \quad (13)$$

where the first RHS term accounts for coagulation of coating monomers with core particles, the second RHS term for the gain by sintering of rough into smooth coating shells and the third RHS term for the gain by surface oxidation of coating precursor vapor. The surface area concentration of smooth coating shells, A_s, is calculated as the area of spheres with the volume of the core particles and smooth coating shells.

2.3.2 Collision diameter of core agglomerates with smooth or rough shells—The coating particles (section 2.2) form fractal-like structures upon deposition on core agglomerates as shown exemplarily in Figure 2a. There the core agglomerate consists of four core primary particles with diameter d_{pc} each having spherical smooth and fractal-like rough coating shells. The collision diameter of these core agglomerates d_c, is calculated at two extreme limiting cases: a) an evenly distributed, spherical coating shell on the core particle (Fig. 2b) or b) a fractal-like particle composed of monodisperse primary particles with equal area and volume.

a. Assuming that smooth and rough shells are evenly and smoothly distributed over the core primary particles, one can calculate by mass balance the enlarged primary particle diameter as the diameter of a sphere with the volume of the initial core primary particle plus its total coating volume of thickness δ (Fig. 2b):

$$d_{pcs}=\left(\left(d_{pc}^3\frac{\pi}{6}+\frac{V_s+V_r}{N_c n_{pc}}\right)\frac{6}{\pi}\right)^{\frac{1}{3}}=d_{pc}+2\delta \quad (14a)$$

The number of core primary particles per core agglomerate, n_{pc}, is calculated by dividing the constant initial number of core primary particles, $N_{c0}n_{pc0}$, by the number of core agglomerates, N_c, accounting for the change in gas volume by cooling:

$$n_{pc}=\frac{N_{c0}n_{pc0}Q_0}{N_c Q} \quad (14b)$$

The smooth shell coated core agglomerate collision diameter, d_{cs}, is (eq. 9):

$$d_{cs}=d_{pcs}n_{pc}^{\frac{1}{D_f}} \quad (14c)$$

b. The fractal-like coated core agglomerate (Fig. 2a) consists of monodisperse primary particles with the same surface area and solid volume as the constituent core particles and coating shells (Fig. 2c). Core primary particles encapsulated with a smooth coating shell are accounted as in eq. 14a for as primary particles with diameter $d_{pc\delta}$, as the diameter of a sphere with the volume of the initial core primary particle plus the smooth coating volume per core primary particle:

$$d_{pc\delta}=\left(\left(d_{pc}^3\frac{\pi}{6}+\frac{V_s}{N_c n_{pc}}\right)\frac{6}{\pi}\right)^{\frac{1}{3}}=d_{pc}+2\delta_s \quad (15a)$$

The monodisperse primary particle diameter, d_{pcr}, of that agglomerate (Fig. 2c) is:

$$d_{pcr}=\frac{6V}{A}=\frac{6\left(N_c n_{pc}d_{pc\delta}^3\frac{\pi}{6}+V_r\right)}{N_c n_{pc}d_{pc\delta}^2\pi+A_r} \quad (15b)$$

where the brackets of the nominator represent the volume of core primary particles plus smooth and rough coating shells. The denominator is the sum of the surface area of the core primary particles encapsulated with the smooth coating shell plus the area of the fractal-like rough coating surface area. The d_{pcr} could be smaller than the core primary particle diameter, d_{pc} (constant), as it accounts for the fractal-like rough coating shell consisting of coating primary particles much smaller than d_{pc}.

The number of monodisperse primary particles, n_{pcr}, is obtained by dividing the volume of core primary particles, the smooth and rough coating shells by the volume of the equivalent monodisperse primary particles d_{pcr}:

$$n_{pcr}=\frac{N_c n_{pc}d_{pc}^3\frac{\pi}{6}+V_s+V_r}{N_c d_{pcr}^3\frac{\pi}{6}} \quad (15c)$$

So the fractal-like shell coated core agglomerate collision diameter is:

$$d_{cr}=d_{pcr}n_{pcr}^{\frac{1}{D_f}} \quad (15d)$$

Here, calculations are carried out for both d_{cs} and d_{cr} to bracket the limits of aerosol coating morphology and dynamics.

2.4 Coating shell characteristics

The total coating thickness, δ, is defined as the thickness of a perfectly smooth and dense coating shell with volume concentration $V_s + V_r$:

$$\delta=\frac{1}{2}\left(\sqrt[3]{\left(\frac{V_s+V_r}{N_c n_{pc}}+d_{pc}^3\frac{\pi}{6}\right)\frac{6}{\pi}}-d_{pc}\right) \quad (16)$$

Similarly the thickness of the smooth coating shell, δ_s, is:

$$\delta_s=\frac{1}{2}\left(\sqrt[3]{\left(\frac{V_s}{N_c n_{pc}}+d_{pc}^3\frac{\pi}{6}\right)\frac{6}{\pi}}-d_{pc}\right) \quad (17)$$

The texture of the coating shell is characterized by the fraction of smooth coating volume concentration of the total coating shell volume concentration, F_{sc}:

$$F_{sc}=\frac{V_s}{V_s+V_r} \quad (18)$$

The coating efficiency, ε, is the fraction of coating precursor vapor that has formed coating shells on core particles:

$$\varepsilon=\frac{(V_s+V_r)\,Q}{C_0 n_m \nu_1 Q_0} \quad (19)$$

2.5 Simulation conditions

The initial temperature of the mixture of core TiO_2 aerosol and HMDSO vapor is $T = 1350$ K (Figure 3, solid line). The temperature decreases with cooling rate $CR = 2\times10^3$ K/s to account for heat losses of the coating reactor (Teleki *et al.*, 2009a). Then the oxidation of HMDSO is completed within $t = 3\times10^{-3}$ s (Fig. 3).

The initial composition of the gas flow is determined by combining the TiO_2 core aerosol, for complete conversion of its precursor, and the HMDSO-laden flow for the standard experiments of Teleki *et al.* (2008). That way the initial composition of the gas flow is 32.5 l/min O_2, 11 l/min CO_2 and 9.7 l/min H_2O and 15.8 l/min HMDSO-laden N_2 at $T = 293$ K. This corresponds to a residence time of $t = 0.1$ s in a tubular reactor with diameter 4.5 cm and a length of 30 cm (Teleki *et al.*, 2009a).

The TiO_2 core particle production rate is always 23.5 g/h and results in an initial single core primary particle ($n_{pc0} = 1$) concentration of $N_{c0} = 4.23\times10^{16}$ #/m^3 at $T = 293$ K for a primary particle size of $d_{pc} = 40$ nm and density $\rho_{TiO2} = 4000$ kg/m^3. The influence of core

particle size at constant production rate is discussed also for d_{pc} = 100 nm and 400 nm corresponding to initial number concentrations of N_{c0} = 2.71×10^{15} and 4.23×10^{13} #/m^3 at T = 293 K, respectively.

The amount of coating is defined by its weight fraction, WF, in the total mass of product (coating and core) particles. With density ρ_{SiO2} = 2200 kg/m^3, WF = 20 wt% SiO_2 corresponds to an initial number concentration of coating precursor vapor of C_0 = 6.63×10^{21}#/m^3 at T = 293 K (HMDSO, n_m = 2).

3. Results and discussion

3.1 Coating particle dynamics

Figure 4 shows the evolution of coating aerosol: a) monomer (N_1, bold lines) and particle (N_2, thin lines) number concentrations and b) primary particle (d_{p2}, bold lines) and collision (d_2, thin lines) diameters for the standard conditions of Teleki *et al.* (2008) d_{pc} = 40 nm and WF = 20 wt%. Results are shown for neglecting (solid and dash-dot lines, α_{max} = 0) and accounting for surface oxidation (dashed lines, α_{max} = 1). The coating thickness was accounted for assuming an evenly distributed smooth shell (eq. 14, solid and dashed lines) and compared with the fractal-like rough shell (eq. 15, dash-dot lines).

When neglecting HMDSO surface oxidation, the monomer concentration decreases slowly until about 0.001 s (Fig. 4a, bold solid line) as monomer generation and loss by coagulation nearly balance each other. Later on (after t = 0.003 s), N_1 decreases quite fast as monomer generation ceases since HMDSO is fully oxidized (Fig. 3, dashed line) and coating monomers grow to particles (N_2) or form smooth shells on the core particles. The N_2 decreases also steadily (Fig. 4a, thin solid line) but slower than N_1 by coagulation with coating particles or core particles to form rough shells.

Accounting for surface oxidation (dashed lines) leads to a faster reduction of N_1 as the gas phase monomer generation competes with oxidation on the surface of core and coating particles (Pratsinis and Spicer, 1998: Fig. 1b). This fast reduction of coating monomer concentration (thick dashed lines) reduces also N_2 (thin dashed lines). The fractal-like texture of the coating shell (dash-dotted line) hardly makes any difference in N_1 and N_2 evolution when surface oxidation is neglected (Fig. 4). It is worth noting, however, that coating particle concentrations converge within about 0.005 s regardless of accounting or not for surface oxidation and the fractal-like structure of the resulting shells on the core particles. Coagulation completely masks all these effects.

Figure 4b shows that when neglecting surface oxidation, the onset of aggregate formation takes place at t = 3×10^{-4} s and that of agglomeration at t = 0.02 s when d_{p2} levels off and sintering stops (Tsantilis and Pratsinis, 2004). The coating primary particles grow faster when accounting for surface oxidation (Pratsinis and Spicer, 1998: Fig. 1a) and reach the onsets of aggregate and agglomerate formation an order of magnitude faster. Nevertheless the coating primary particle size at the onset of aggregate formation is not much influenced by surface oxidation as well as the final coating primary and collision diameters. This indicates that a more accurate description of the surface reaction may not change considerably the predicted particle sizes at the employed process conditions (e.g. temperature and concentrations). The final primary particle diameter is 4 nm in coating agglomerates with a collision diameter of 65 nm. Accounting for fractal-like rough shells (eq. 15, dash-dotted line) makes hardly any difference in coating primary particles size and decreases slightly the coating agglomerate size. Apparently accounting for the fractal shells on the core particles leads to smaller coating agglomerates by more effective scavenging of

coating particles with core particles, accelerating the increase of coating efficiency as it will be shown next.

3.2 Coating shell characteristics

Figure 5 shows the evolution of a) coating efficiency, ε (bold lines), and fraction of smooth coating, F_{sc} (thin lines), and b) total, δ (bold lines), and smooth, δ_s (thin lines), coating thickness for the conditions of Figure 4, neglecting (solid and dash-dot lines, $\alpha_{max} = 0$) and accounting for surface oxidation (dashed lines, $\alpha_{max} = 1$). The coating thickness was accounted for assuming core particles with evenly distributed smooth (eq. 14, solid and dashed lines) or fractal-like rough coating shells (eq. 15, dash-dot lines).

As coating takes place, coating monomers and particles deposit on the surface of core particles increasing steadily the coating efficiency, ε. Early on, the fraction of smooth coating, F_{sc}, is 100 % as the shell is formed primarily by coating monomers and small coating particles (clusters) that sinter fast into smooth coating shells. Later on, F_{sc} decreases as soon as coating particles start to form aggregates (Fig. 4b) at $t = 3\times10^{-4}$ s (solid line). Then, sintering becomes too slow to smooth out the coating shell. Finally, F_{sc} approaches a constant value as soon as ε approaches 100 % and the coating process is completed. Figure 5b shows that coating thickness increases quite fast. At the onset of (coating) aggregate formation ($t = 3\times10^{-4}$ s, Fig. 4b), δ increases faster than δ_s in agreement with the decreasing fraction of smooth coating (Fig. 5a). It can be seen that the smooth coating thickness, δ_s, reaches the final value quite early, at $t = 2\times10^{-3}$ s. This happens because the concentration of coating monomers N_1 (which form smooth coating shells) decreases rapidly at that time (Fig. 4a).

Accounting for surface oxidation reduces drastically the fraction of smooth coatings, F_{sc}, and coating efficiency, ε, which is a counterintuitive result (dashed lines). The total coating thickness increases slower but nearly to the same value as without surface oxidation. The smooth coating thickness is practically zero as only rough coatings are found. What happens? The core TiO_2 particles compete for coating precursor molecules with the newly formed SiO_2 coating particles. As the latter have much larger surface area than the core particles, large coating particles form resulting in aggregates quite early ($t = 2\times10^{-5}$ s) that stop sintering at $t = 10^{-3}$ s (Fig. 4b).

Although the detailed reaction kinetics for gas phase and in particular for surface oxidation of HMDSO are unknown and had to be approximated, a clear trend emerges: if HMDSO surface oxidation competes effectively with its gas phase oxidation, there is little chance for synthesis of smooth coatings at the employed process conditions. As rather smooth coating shells were obtained experimentally at these conditions (Teleki *et al.*, 2008), the effect of surface oxidation is neglected in subsequent calculations as the surface reaction rate of HMDSO is really unknown and perhaps rather small at the employed conditions, but not necessarily zero. For example, surface growth of HMDSO is driving growth of SiO_2 nanofibers or nanowires in flame deposition of antifogging silica films on glass substrates at low HMDSO concentrations (Tricoli *et al.*, 2009). Similarly, the SiO_2 sintering rate employed here (Tsantilis *et al.*, 2001) was compared to that by Xiong *et al.* (1993). The latter gave much lower coating efficiencies and rougher coating in contrast to experimental data (Teleki *et al.*, 2008). As a result, the sintering rate of Tsantilis *et al.* was used in all simulations.

Accounting for the fractal-like structure of rough coating shells (dash-dot lines) accelerates the evolution of both ε (Fig. 5a) and δ (Fig. 5b) by higher coagulation rates but reach the same asymptotic values as when neglecting it (solid lines). This can be seen also by the slightly lower coating particle concentration (N_2) at higher residence times in Fig. 4a (dash-

dot lines). The fraction of smooth coating attains a slightly higher value than the evenly distributed coating shells (solid line). Perhaps, fractal-like structures scavenge more efficiently coating SiO_2 monomers up to about $t = 0.001$ s (Fig. 4a,b).

3.3 Effect of core particle diameter and coating vapor concentration

Figure 6 shows the evolution of a) N_1 (bold lines) and N_2 (thin lines) and b) d_{p2} (bold lines) and d_2 (thin lines) for lower coating weight fraction, $WF = 5$ wt% (dashed lines), with $d_{pc} = 40$ nm and bigger core primary particles $d_{pc} = 100$ (dash-dot lines) or 400 nm (dotted lines), but with $WF = 20$ wt% and neglecting surface oxidation, accounting for evenly distributed coating shells (eq. 14). Lowering the WF (dashed lines) leads to generation of less coating monomers that result in lower N_1 and N_2. At the same WF, increasing the core primary particle size and therefore decreasing the number concentration of core particles hardly affects N_1 and N_2 that are nearly identical to those of Fig. 4a (solid lines).

Figure 6b shows that less coating material, $WF = 5$ wt%, leads to slower coating particle growth, with slightly smaller primary particles but amazingly little aggregate and agglomerate formation. This is caused by slower coagulation rates arising from lower particle concentrations (Fig. 6a). At higher $WF = 20$ wt%, increasing the core primary particle size (d_{pc}) leads to coating agglomerates with slightly higher collision diameter, but identical primary particles size. Larger core primary particles offer less area for coating monomer and particle deposition. As a result, more coating material remains in the gas phase to coagulate into larger coating agglomerates.

Figure 7 shows the evolution of coating characteristics for $WF = 5$ wt% for $d_{pc} = 40$ nm (dashed lines) and $WF = 20$ wt% for $d_{pc} = 100$ (dash-dot lines) and 400 nm (dotted lines) neglecting surface oxidation, all accounting for evenly distributed coating shells (eq. 14). Decreasing the WF to 5 wt% for $d_{pc} = 40$ nm accelerates the attainment of maximum of coating efficiency (Fig. 7a). Increasing the core particle size to 100 and 400 nm reduces the coating efficiency below that of 40 nm core primary particles (Fig. 7a) by the lower core particle number and area concentrations for deposition. The fraction of smooth coating decreases as soon as coating particles start to form aggregates at $t = 3\times10^{-4}$ s for $d_{pc} = 100$ and 400 nm (Fig. 7). For $WF = 5$ wt% only a small amount of intermediate rough coating shells is formed decreasing the fraction of smooth coating to 95 % between $t = 10^{-3}$ - 10^{-2} s in agreement with the short duration of aggregate formation (Fig 6b).

Figure 7b shows that for $WF = 5$ wt% the total and smooth coating thickness are identical at about 0.6 nm, corresponding to a coating monolayer and consistent with the limited formation of aggregates (Fig. 6b). At constant core particle production rate, increasing the core particle diameter slightly increases the smooth coating thickness, but most of the coating texture is quite rough with low coating efficiency as most coating material has formed SiO_2 particles rather than shells onto the core TiO_2 particles. It is worth noting, however, that at WF = 20 wt% for $d_{pc} = 400$ nm the F_{sc} is higher (Fig. 7a, dotted line) than that for $d_{pc} = 100$ nm (Fig. 7a, das-dotted line) and even higher than that for 40 nm (Fig. 5a, solid line) at $t = 0.1$ s. This paradox is attributed to formation of large coating particles that hardly reach the core particles, resulting in a really low coating efficiency (Fig. 7a, dotted line). As a result, one may obtain a higher fraction of smooth shells but at reduced and probably unacceptable process yield (coating efficiency, ε).

3.4 Coating diagrams and comparison with experimental data

Figure 8 shows a) coating efficiency and b) fraction of smooth coating in the parameter space of core primary particle diameter, d_{pc}, and coating weight fraction, WF, at constant core particle production rate and coating reactor residence time $t = 0.1$ s. Following the

analysis above, only evenly distributed coating shells (eq. 14) have been considered and surface oxidation of HMDSO has been neglected as these assumptions do not alter the product characteristics considerably. The white contours represent the total, δ (Fig. 8a), and smooth coating thickness, δ_s (Fig. 8b). The WF ranges from 1 to 50 wt% corresponding to a mole Si/Ti = 0.013 - 0.66 that experimentally seems to give good coating characteristics (Akhtar *et al.*, 1992; Hung and Katz, 1992; Powell *et al.*, 1997a,b; Teleki *et al.*, 2005, 2008, 2009b).

Increasing the core particle diameter d_{pc} at constant core particle production rate does not affect coating efficiency (Fig. 8a) up to d_{pc} = 100 nm. At these conditions, coagulation of coating particles is fast enough to let all coating material deposit onto the core particles, resulting in perfect coating efficiencies (ε = 100 %, red). Larger d_{pc}, however, lower the ε (blue) because the coagulation rate between core and coating particles is reduced by the low concentration of core particles. The coating weight fraction, WF, weakly influences ε in the investigated range (Fig. 8a). This weak influence can be explained by the corresponding small variation in coating precursor vapor concentration compared to the variation in N_c by changing d_{pc}. Increasing d_{pc} by a factor of 10 reduces N_{c0} by 1000 at constant core particle production rate and therefore lowers the core particle surface area concentration by a factor of 10. For low WF the range for d_{pc} to achieve high coating efficiencies is slightly increased.

Increasing WF leads to proportionally increasing total coating thickness (white contours), depending on coating efficiency. This is consistent with Boies *et al.* (2009) who found that the coating precursor flow rate and nitrogen purge gas dilution influenced the coating thickness the most in their reactor. Up to d_{pc} = 100 nm, the total coating thickness increases with d_{pc} as the surface area concentration of core particles is decreasing with increasing d_{pc} and ε = 100 % (red). Above 100 nm, δ decreases with the decreasing coating efficiency, ε.

The fraction of smooth coating, F_{sc}, reaches up to 100 % (red) for small d_{pc} and low WF (Fig. 8b) where most of the shell is deposited by the coating monomers and small clusters at the high coagulation rates. The apparent minimum of δ and F_{sc} (blue) is attributed to the formation of aggregates and the decreasing coagulation rates of core particles with coating particles as discussed in Figure 7. Higher WF lead to more coating particles while larger d_{pc} decrease the coagulation rate of coating with core particles, both promoting the formation of coating aggregates that finally lead to rough shells (Fig. 4b and 5a). For the largest d_{pc} barely any shells are deposited by coagulation with coating particles within the reactor residence time while coagulation with coating monomers early in the process still leads to thin smooth shells. The thickness of these smooth shells shows a weaker dependence on d_{pc} than the total thickness. This faster decrease of the deposited amount of rough shells than that of smooth shells leads to an increase of F_{sc} after the minimum for increasing d_{pc}. In Figure 8a it can be seen that these smoother shells at the largest d_{pc} come, however, at fairly low coating efficiencies, which means low and perhaps unacceptable process yields.

The circles in Figure 8 correspond to the experimental conditions of Teleki *et al.* (2008) where spherical TiO_2 core particles with a diameter of 40 nm were coated with WF = 5, 10 and 20 wt% of SiO_2 and high ε were reported (few separate SiO_2 particles in the product), which is consistent with the above diagrams. The total and smooth coating thickness are increasing and the fraction of smooth coating shells is decreasing for increasing WF consistent with Teleki *et al.* (2008). More specifically, for WF = 20 wt% the simulation results in total and smooth coating thicknesses between 2 to 3 nm and 0.7 to 0.8 nm, respectively and coating shells with F_{sc} = 30 %. This is in agreement with Teleki *et al.* (2008) who reported a total coating thickness of 2 nm with rather rough surface texture at these conditions. This dependency of F_{sc} on WF is consistent also with Hung and Katz (1992), who reported that increasing the precursor concentration ratio (increasing Si/Ti or

WF) led to less uniform coating thickness distribution on the same core particle. For low concentrations of SiO_2 precursor vapor, they observed discrete spots of SiO_2 on TiO_2 core particles. The diagram is also consistent with Powell *et al.* (1997a,b) who found that increasing the coating precursor vapor concentration led to rougher coatings.

The lower $WF = 5$ wt % leads to thinner coating shells with a thickness a little above 0.4 nm corresponding to a monolayer of coating monomers, too thin to be detected by microscopy and without any rough coatings! The presence of such a thin SiO_2 shell is consistent again with Teleki *et al.* (2008) who observed 50% reduction of photo-oxidation of isopropanol to acetone and attributed this to partially-coated particles. The thickness and completeness of these totally smooth coating shells could be increased by multiple injection of precursor vapor of low *WF* in series building up coating shells layer-by-layer along the aerosol reactor similar to atomic layer deposition processes (King *et al.*, 2008).

4. Conclusions

A trimodal model for high temperature aerosol coating was developed accounting for gas phase oxidation, coagulation, sintering and surface growth. Coating of TiO_2 aerosol nanoparticles with nanothin SiO_2 shells by hexamethyldisiloxane (HMDSO) vapor oxidation was investigated predicting the coating thickness, texture and efficiency in terms of design diagrams that were consistent with pertinent experimental data.

Smooth coatings were formed primarily by deposition of freshly-formed SiO_2 monomers and sintering of small SiO_2 clusters and to a much lesser extent by surface oxidation of HMDSO on the TiO_2 core particles. Accounting for surface oxidation by a two-step model in the absence of an overall reaction rate, resulted in rough coating shells at the employed process conditions. This was in contrast to pertinent experimental data indicating the minimal significance of surface reaction here. Accounting also for the structure of shells (rough fractal-like or smooth) had a little influence on the design calculations at the present process conditions.

The concentrations of core aerosol and coating precursor vapor (here HMDSO) had the strongest influence on coating efficiency and shell texture in agreement with the literature. Bigger core particles at constant production rate lead to lower coating efficiency. Increasing the coating weight fraction hardly influences the coating efficiency and leads to proportionally higher total coating thickness but also to rougher coating shells. Low concentrations of coating precursor vapor and high concentrations of core particles lead to high fractions of smooth shells and high coating efficiency. The thickness of these smooth shells could be increased by multiple injections of coating precursor vapor at low concentrations in series, building up smooth coating shells layer-by-layer.

Acknowledgments

Financial support from Swiss National Science Foundation (SNF) grant # 200021-119946/1 and European Research Council is gratefully acknowledged.

Appendix

Sintering reduces the rough coating shell surface area, A_r, and volume, V_r, concentration. For a perfectly smooth and fully coalesced coating no rough coating exists and therefore A_r and V_r, converge to zero. As a result the entire rough coating film area concentration is the driving power for sintering, while the kinetics are given by the characteristic sintering time (Tsantilis *et al.*, 2001), $\tau(d_{pr})$:

$$\left.\frac{dA_r}{dt}\right|_{sintering} = -\frac{(A_r - 0)}{\tau\left(d_{pr}\right)} = -\frac{A_r}{\tau\left(d_{pr}\right)} \quad \text{(A1)}$$

As rough coating shells become smooth by sintering, its volume concentration decreases as follows:

$$\left.\frac{dV_r}{dt}\right|_{sintering} = -\frac{V_r}{\tau\left(d_{pr}\right)} \quad \text{(A2)}$$

The gain in smooth coating volume is given by the overall volume balance:

$$\left.\frac{dV_s}{dt}\right|_{sintering} = -\left.\frac{dV_r}{dt}\right|_{sintering} \quad \text{(A3)}$$

6. Nomenclature

A_r	surface area concentration of rough coating shell	[$m^2\ m^{-3}$]
A_s	surface area concentration of smooth coating shell	[$m^2\ m^{-3}$]
A_2	surface area concentration of coating particles	[$m^2\ m^{-3}$]
a_1	surface area of coating monomer	[m^2]
a_2	surface area of coating particle	[m^2]
a_{2f}	surface area of fully-coalesced (spherical) coating particle	[m^2]
C	coating precursor vapor concentration	[# m^{-3}]
C_0	initial coating precursor vapor concentration	[# m^{-3}]
CR	cooling rate	[K s^{-1}]
D_f	fractal dimension	[-]
d_2	collision diameter of coating particle	[m]
d_{cs}	collision diameter of core particle (smooth)	[m]
d_{cr}	collision diameter of core particle (fractal-like)	[m]
d_{pc}	primary particle diameter of core particle	[m]
d_{pcr}	equivalent primary particle diameter of core agglomerate coated with rough shells	[m]
d_{pcs}	diameter of core primary particle (smooth)	[m]
$d_{pc\delta}$	diameter of core primary particle with smooth coating shell (fractal-like)	[m]
$d_{p,min}$	minimum sintering primary particle diameter	[m]
d_{pr}	primary particle diameter of rough coating shell	[m]
d_{p2}	primary particle diameter of coating particle	[m]
F_{sc}	fraction of smooth coating shells	[%]
k	overall oxidation rate constant	[s^{-1}]
k_g	gas phase oxidation rate constant	[s^{-1}]
k_s	overall surface oxidation rate constant	[s^{-1}]
N_1	number concentration of coating monomers	[# m^{-3}]
N_2	number concentration of coating particles	[# m^{-3}]
N_c	number concentration of core particles	[# m^{-3}]

Europe PMC Funders Author Manuscripts

N_{c0}	initial number concentration of core particles	[# m^{-3}]
n_m	number of monomers per precursor molecule	[-]
n_{p2}	number of primary particles per coating particle	[-]
n_{pc}	number of core primary particles per core particle	[-]
n_{pc0}	initial number of core primary particles per core particle	[-]
n_{pcr}	number of equivalent primary particles per core agglomerate coated with rough shells	[-]
Q	gas flow rate	[m^3 s^{-1}]
Q_0	initial gas flow rate	[m^3 s^{-1}]
r	volume ratio, $r = v_2/v_1$	[-]
T	temperature	[K]
t	residence time	[s]
V_r	volume concentration of rough coating shells	[m^3 m^{-3}]
V_s	volume concentration of smooth coating shells	[m^3 m^{-3}]
V_2	volume concentration of coating particles	[m^3 m^{-3}]
v_1	volume of coating monomer	[m^3]
v_2	volume of coating particle	[m^3]
WF	weight fraction of coating material	[%]

6.1 Greek Letters

α	fraction of collisions leading to surface oxidation	[-]
β	collision frequency	[m^3 s^{-1}]
δ	total coating thickness	[m]
δ_s	smooth coating thickness	[m]
ϵ	coating efficiency	[%]
ρ_{SiO2}	density of SiO_2	[kg m^{-3}]
ρ_{TiO2}	density of TiO_2	[kg m^{-3}]
τ	characteristic sintering time	[s]

References

Akhtar MK, Pratsinis SE, Mastrangelo SVR. Dopants in Vapor-Phase Synthesis of Titania Powders. J. Am. Ceram. Soc. 1992; 75:3408–3416.

Boies AM, Roberts JT, Girshick SL, Zhang B, Nakamura T, Mochizuki A. SiO_2 coating of silver nanoparticles by photoinduced chemical vapor deposition. Nanotechnology. 2009; 20:295604. [PubMed: 19567950]

Clark, HB.; Long, JS. Titanium dioxide pigments. In: Myers, PR., editor. Treatise on Coatings, 3, Pigments Part I. Marcel Dekker; New York: 1975. p. 479-532.

Egerton TA. The Modification of Fine Powders by Inorganic Coatings. KONA Powder and Particles. 1998:16.

Ehrman SH, Friedlander SK, Zachariah MR. Characteristics of SiO_2/TiO_2 nanocomposite particles formed in a premixed flat flame. J. Aerosol Sci. 1998; 29:687–706.

Fisher J, Egerton TA. Titanium compounds, Inorganic, Kirk-Othmer Encyclopedia of Chemical Technology (Electronic Edition). John Wiley & Sons, Inc. 2001

Fotou GP, Pratsinis SE, Baron PA. Coating of silica fibers by ultrafine particles in a flame reactor. Chem. Eng. Sci. 1994; 49:1651–1662.

Friedlander, SK. second ed. Oxford University Press; New York: 2000. Smoke, Dust and Haze: Fundamentals of Aerosol Dynamics.

Friedlander SK, Wu MK. Linear rate law for the decay of the excess surface area of a coalescing solid particle. Physical Review B. 1994; 49:3622.

Heine MC, Pratsinis SE. High concentration agglomerate dynamics at high temperatures. Langmuir. 200622:10238–10245. [PubMed: 17107027]

Hung CH, Katz JL. Formation of mixed-oxide powders in flames .1. TiO_2-SiO_2. J. Mater. Res. 1992; 7:1861–1869.

Jain S, Fotou GP, Kodas TT. A theoretical study on gas-phase coating of aerosol particles. J. Colloid Interface Sci. 1997; 185:26–38. [PubMed: 9056293]

Jeong JI, Choi M. A simple bimodal model for the evolution of non-spherical particles undergoing nucleation, coagulation and coalescence. J. Aerosol Sci. 2003; 34:965–976.

Jeong JI, Choi M. A bimodal particle dynamics model considering coagulation, coalescence and surface growth, and its application to the growth of titania aggregates. J. Colloid Interface Sci. 2005; 281:351–359. [PubMed: 15571690]

King DM, Liang X, Burton BB, Akhtar MK, Weimer AW. Passivation of pigment-grade TiO_2 particles by nanothick atomic layer deposited SiO_2 films. Nanotechnology. 2008; 19:255604. [PubMed: 21828656]

Koch W, Friedlander SK. The effect of particle coalescence on the surface area of a coagulating aerosol. J. Colloid Interface Sci. 1990; 140:419–427.

Kruis FE, Kusters KA, Pratsinis SE, Scarlett B. A simple-model for the evolution of the characteristics of aggregate particles undergoing coagulation and sintering. Aerosol Science and Technology. 1993; 19:514–526.

Mezey, EJ. Jr. Wiley; New York: 1966. Pigments and Reinforcing Agents.

Powell QH, Fotou GP, Kodas TT, Anderson BM. Synthesis of alumina- and alumina/silica-coated titania particles in an aerosol flow reactor. Chem. Mater. 1997a; 9:685–693.

Powell QH, Fotou GP, Kodas TT, Anderson BM, Guo YX. Gas-phase coating of TiO_2 with SiO_2 in a continuous flow hot-wall aerosol reactor. J. Mater. Res. 1997b; 12:552–559.

Pratsinis SE, Mastrangelo SVR. Material Synthesis in Aerosol Reactors. Chem. Eng. Prog. 1989; 85:62–66.

Pratsinis SE, Spicer PT. Competition between gas phase and surface oxidation of $TiCl_4$ during synthesis of TiO_2 particles. Chem. Eng. Sci. 1998; 53:1861–1868.

Schaefer DW, Hurd AJ. Growth and Structure of Combustion Aerosols: Fumed Silica. Aerosol Sci. Technol. 1990; 12:876–890.

Sheen S, Yang S, Jun K, Choi M. One-step flame method for the synthesis of coated composite nanoparticles. Journal of Nanoparticle Research. 2009; 11:1767–1775.

Subramanian, NS.; Diemer, RB.; Gai, PL. E. I. du Pont de Nemours and Company. Wilmington, DE, US: 2006. Process for making durable rutile titanium dioxide pigment by vapor phase deposition of surface treatment. U.S. Patent 200627303(A1)

Teleki A, Buesser B, Heine MC, Krumeich F, Akhtar MK, Pratsinis SE. Role of Gas-Aerosol Mixing during in Situ Coating of Flame-Made Titania Particles. Industrial & Engineering Chemistry Research. 2009a; 48:85–92.

Teleki A, Heine MC, Krumeich F, Akhtar MK, Pratsinis SE. *In-situ* coating of flame-made TiO_2 particles by nanothin SiO_2 films. Langmuir. 2008; 24:12553–12558. [PubMed: 18850688]

Teleki A, Pratsinis SE, Wegner K, Jossen R, Krumeich F. Flame-coating of titania particles with silica. J. Mater. Res. 2005; 20:1336–1347.

Teleki A, Suter M, Kidambi PR, Ergeneman O, Krumeich F, Nelson BJ, Pratsinis SE. Hermetically Coated Superparamagnetic Fe_2O_3 Particles with SiO_2 Nanofilms. Chemistry of Materials. 2009b; 21:2094–2100.

Tricoli A, Righettoni M, Pratsinis SE. Anti-Fogging Nanofibrous SiO_2 and Nanostructured SiO_2-TiO_2 Films Made by Rapid Flame Deposition and In Situ Annealing. Langmuir. 2009; 25:12578–12584. [PubMed: 19621912]

Tsantilis S, Briesen H, Pratsinis SE. Sintering time for silica particle growth. Aerosol Sci. Technol. 2001; 34:237–246.

Tsantilis S, Kammler HK, Pratsinis SE. Population balance modeling of flame synthesis of titania nanoparticles. Chemical Engineering Science. 2002; 57:2139–2156.

Tsantilis S, Pratsinis SE. Soft- and hard-agglomerate aerosols made at high temperatures. Langmuir. 2004; 20:5933–5939. [PubMed: 16459612]

Ulrich GD. Theory of Particle Formation and Growth in Oxide Synthesis Flames. Combust. Sci. Technol. 1971; 4:47–57.

Wegner K, Stark WJ, Pratsinis SE. Flame-nozzle synthesis of nanoparticles with closely controlled size, morphology and crystallinity. Mater. Lett. 2002; 55:318–321.

Xiong Y, Akhtar MK, Pratsinis SE. Formation of agglomerate particles by coagulation and sintering--Part II. The evolution of the morphology of aerosol-made titania, silica and silica-doped titania powders. J. Aerosol Sci. 1993; 24:301–313.

Xiong Y, Pratsinis SE. Gas-phase production of particles in reactive turbulent flows. J. Aerosol Sci. 1991; 22:637–655.

Europe PMC Funders Author Manuscripts

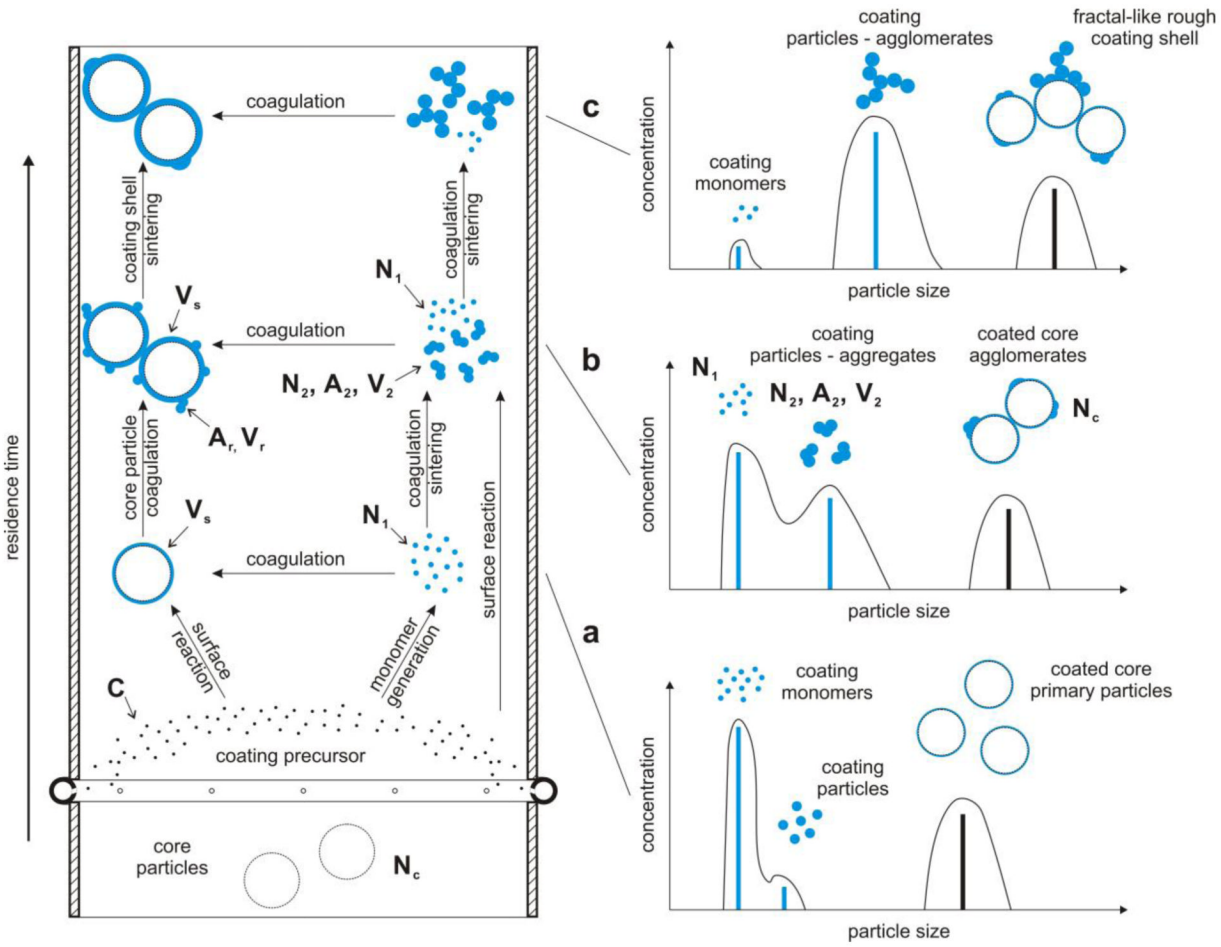

Figure 1.

Schematic of the coating process (left) and the corresponding evolution of the trimodal particle size distribution (right): a) formation of coating monomers and particles as well as smooth shells on the core particles from conversion of the corresponding precursor vapor, b) end of coating precursor vapor conversion and growth of coating particles into aggregates and rough and smooth shells, c) formation of coating agglomerates and fractal-like coating shells.

Europe PMC Funders Author Manuscripts

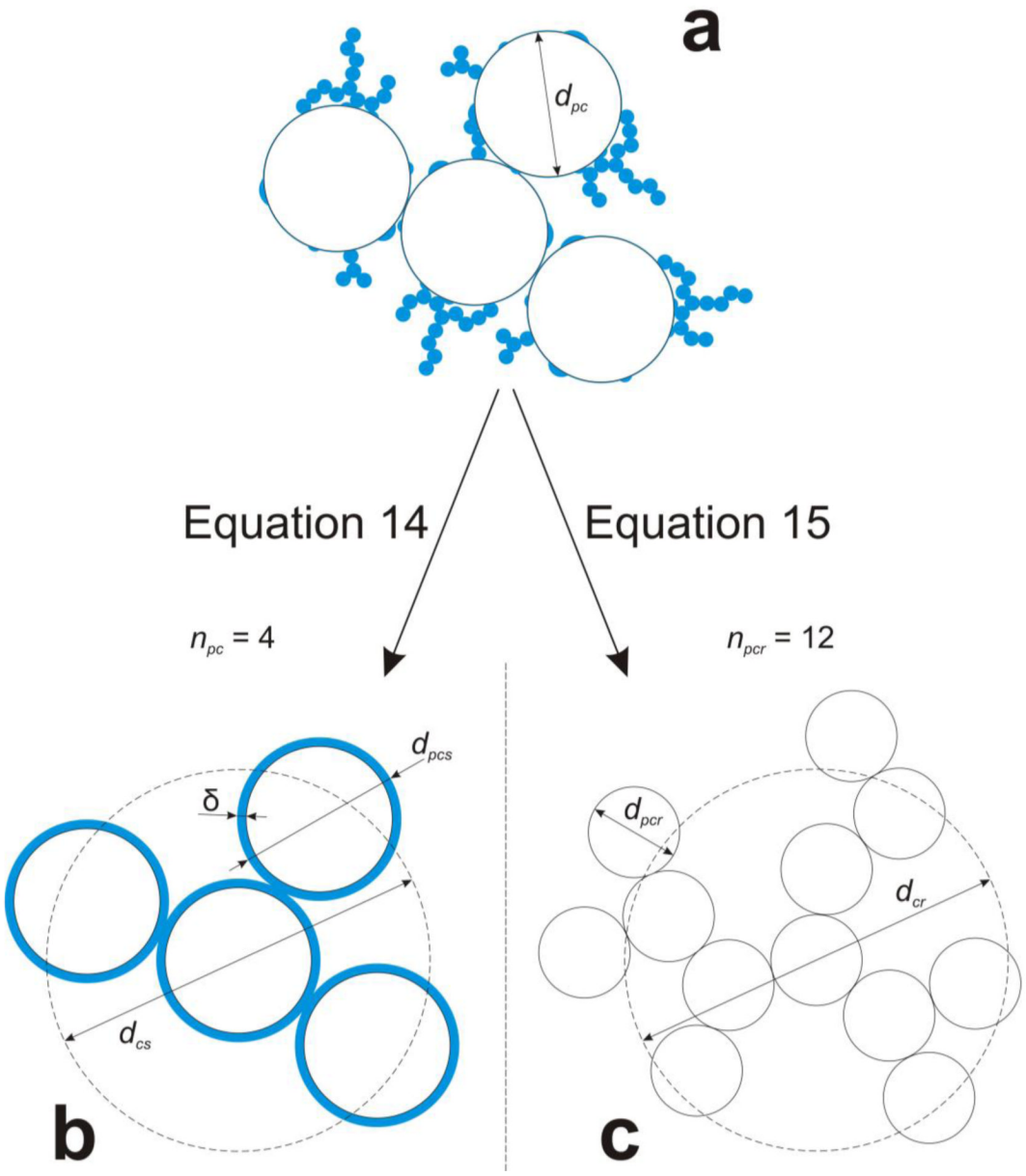

Figure 2.
Schematic of two limiting cases for calculation of the collision diameter of a fractal-like coated core agglomerate (a) having original core primary particle diameter d_{pc}: b) d_{cs} when accounting for the deposited coating as evenly distributed smooth shells with total thickness δ. So, its new primary particle diameter is $d_{pcs} = d_{pc} + 2\delta$. c) d_{cr} when describing the core agglomerate and fractal-like coating as one agglomerate with equal surface area and volume consisting of n_{pcr} equivalent monodisperse primary particles of diameter d_{pcr}.

Europe PMC Funders Author Manuscripts

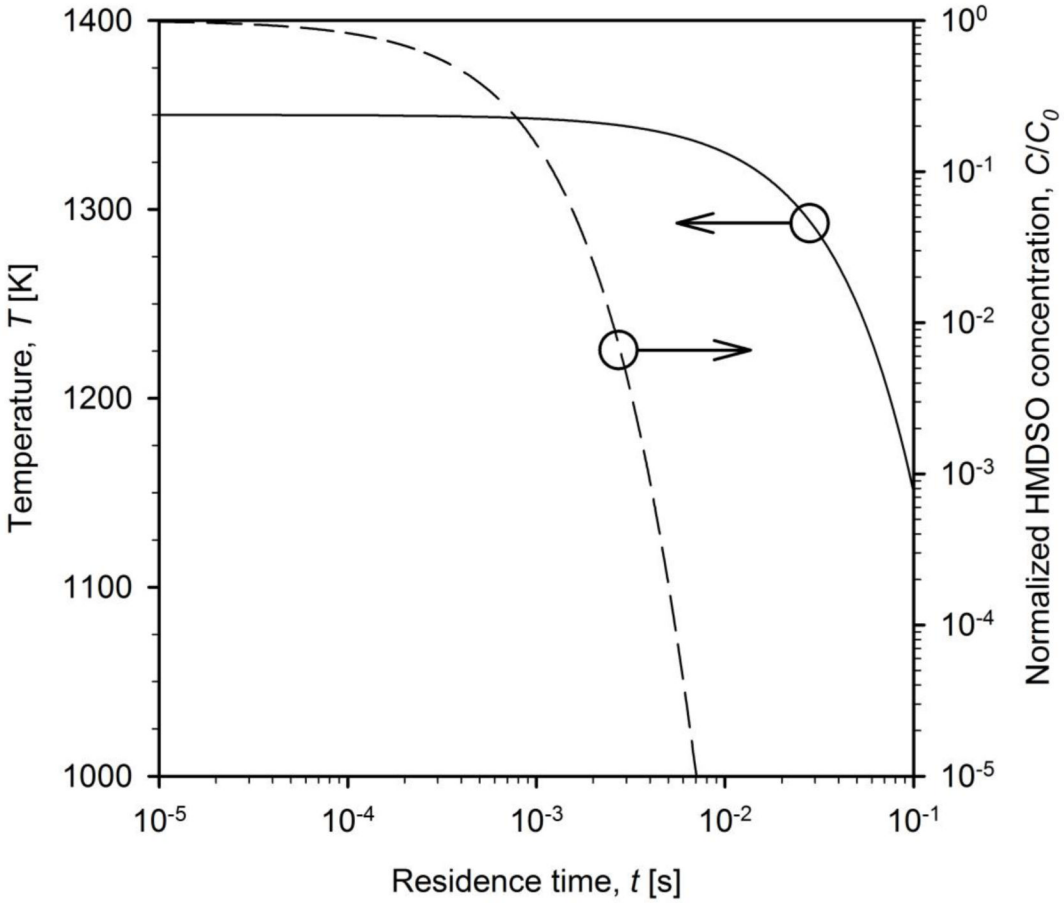

Figure 3.
The evolution of temperature (solid line) and normalized HMDSO concentration (dashed line) as function of residence time inside the coating reactor. The initial temperature T = 1350 K decreases with cooling rate $CR = 2\times10^3$ K/s (Teleki *et al.* 2009a).

Europe PMC Funders Author Manuscripts

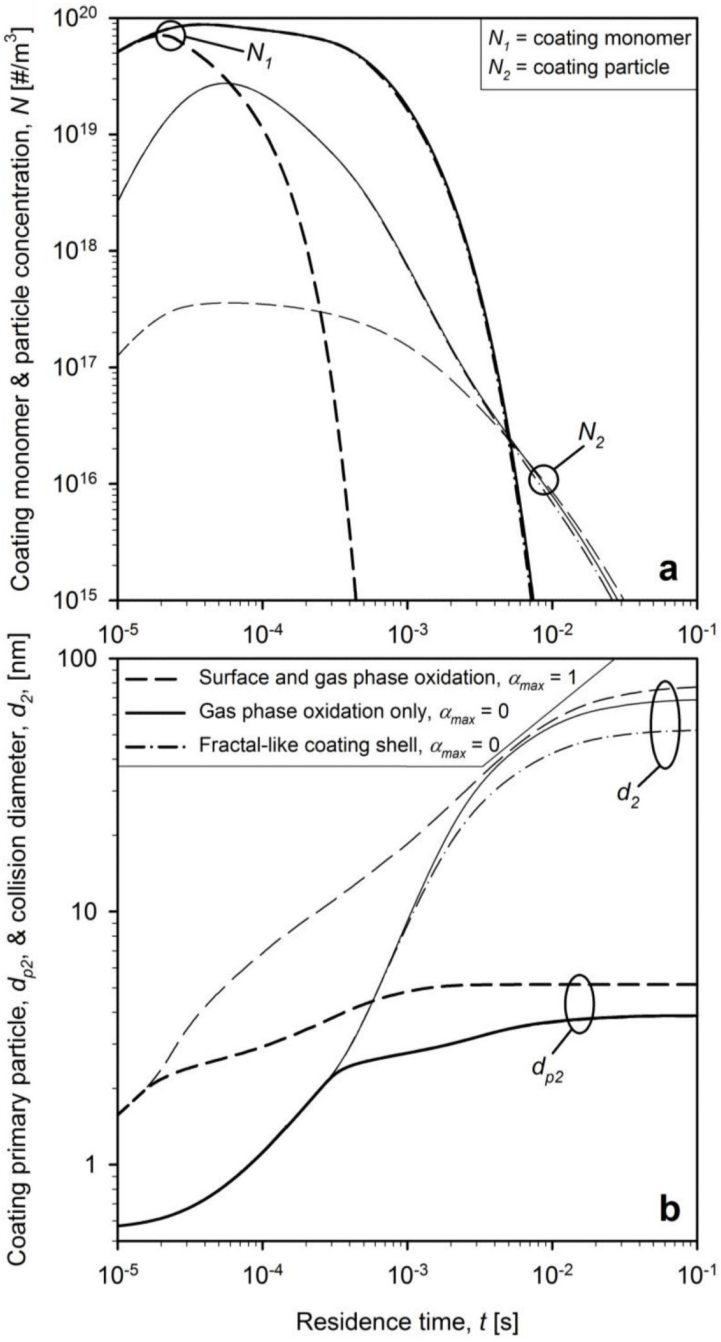

Figure 4.

The evolution of a) number concentration of coating monomers (bold lines) and particles (thin lines) and b) primary particle (bold lines) and collision (thin lines) diameter of coating particles for d_{pc} = 40 nm and WF = 20 wt% for neglecting (solid and dash-dot lines) and accounting for HMDSO surface oxidation (dashed lines). Collision diameters are calculated with assuming smooth shells (solid and dashed lines) and fractal-like rough shells (dash-dot lines).

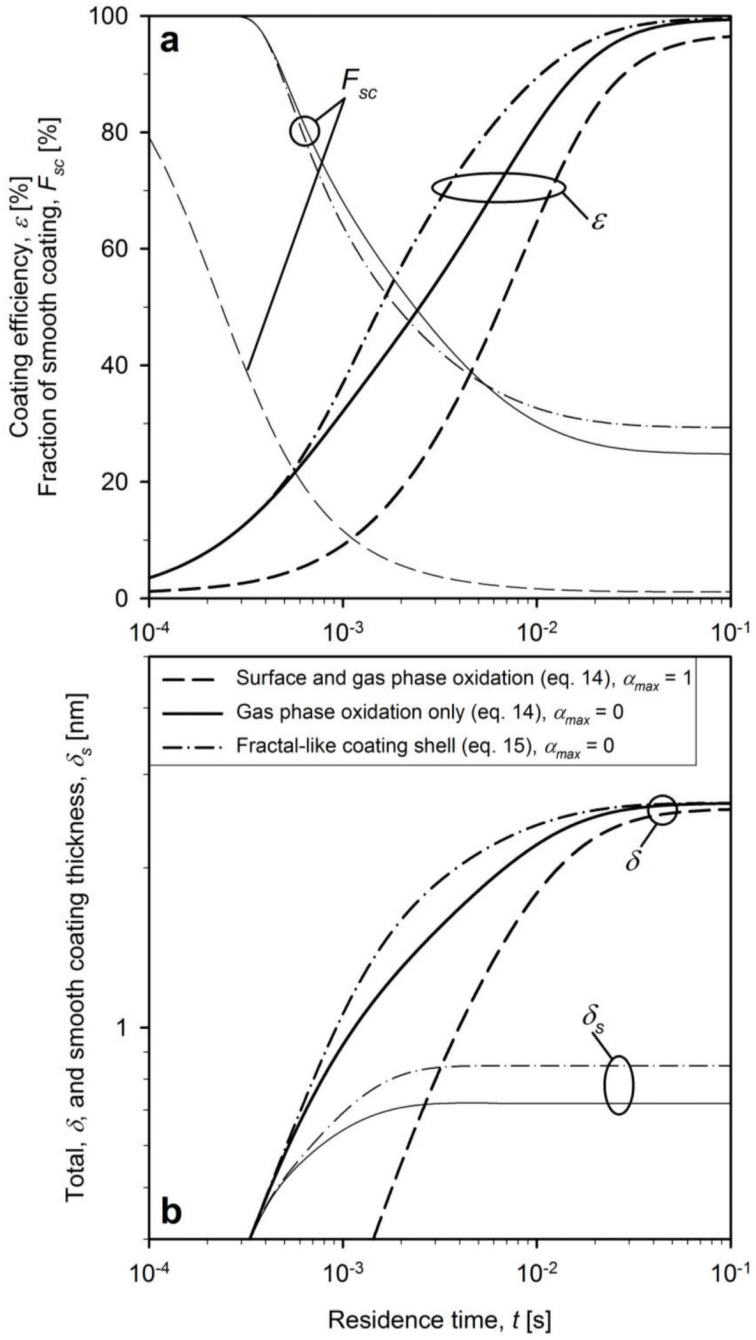

Figure 5.

The evolution of a) coating efficiency (bold lines) and fraction of smooth coating (thin lines) and b) total (bold lines) and smooth (thin lines) coating thickness for d_{pc} = 40 nm and WF_{SiO2} = 20 wt% for neglecting (solid and dash-dot lines) and accounting for HMDSO surface oxidation (dashed lines). Collision diameters are calculated assuming smooth (solid and dashed lines) or fractal-like rough shells (dash-dot lines).

Europe PMC Funders Author Manuscripts

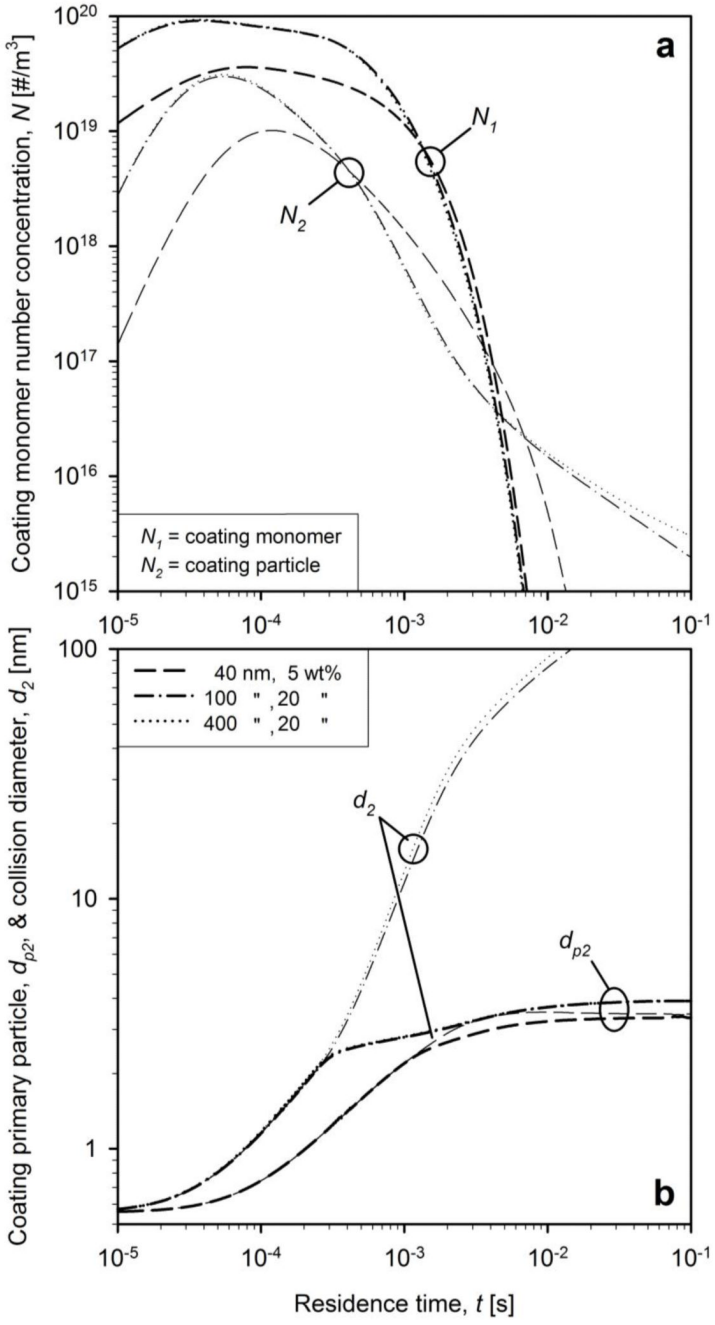

Figure 6.

The evolution of a) number concentration of coating monomers (bold lines) and particles (thin lines) and b) primary particle (bold lines) and collision (thin lines) diameter of coating particles for d_{pc} = 40 nm and WF = 5 wt% (dashed lines), as well as WF = 20 wt% and d_{pc} = 100 (dash-dot lines) and 400 nm (dotted lines).

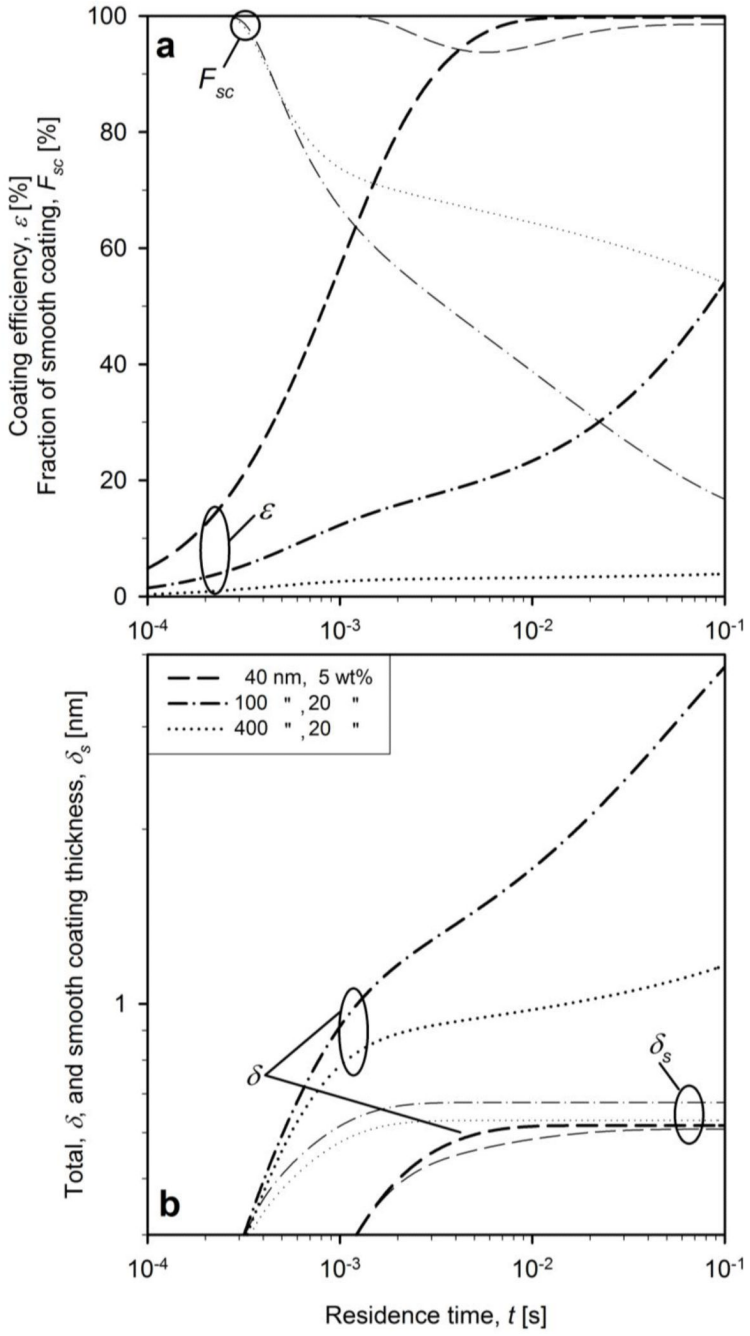

Figure 7.

The evolution of a) the coating efficiency (bold lines) and fraction of smooth coating (thin lines) and b) the evolution of total (bold lines) and smooth (thin lines) coating thickness for d_{pc} = 40 nm and WF = 5 wt% (dashed lines), as well as WF = 20 wt% and d_{pc} = 100 (dash-dot lines) and 400 nm (dotted lines).

Europe PMC Funders Author Manuscripts

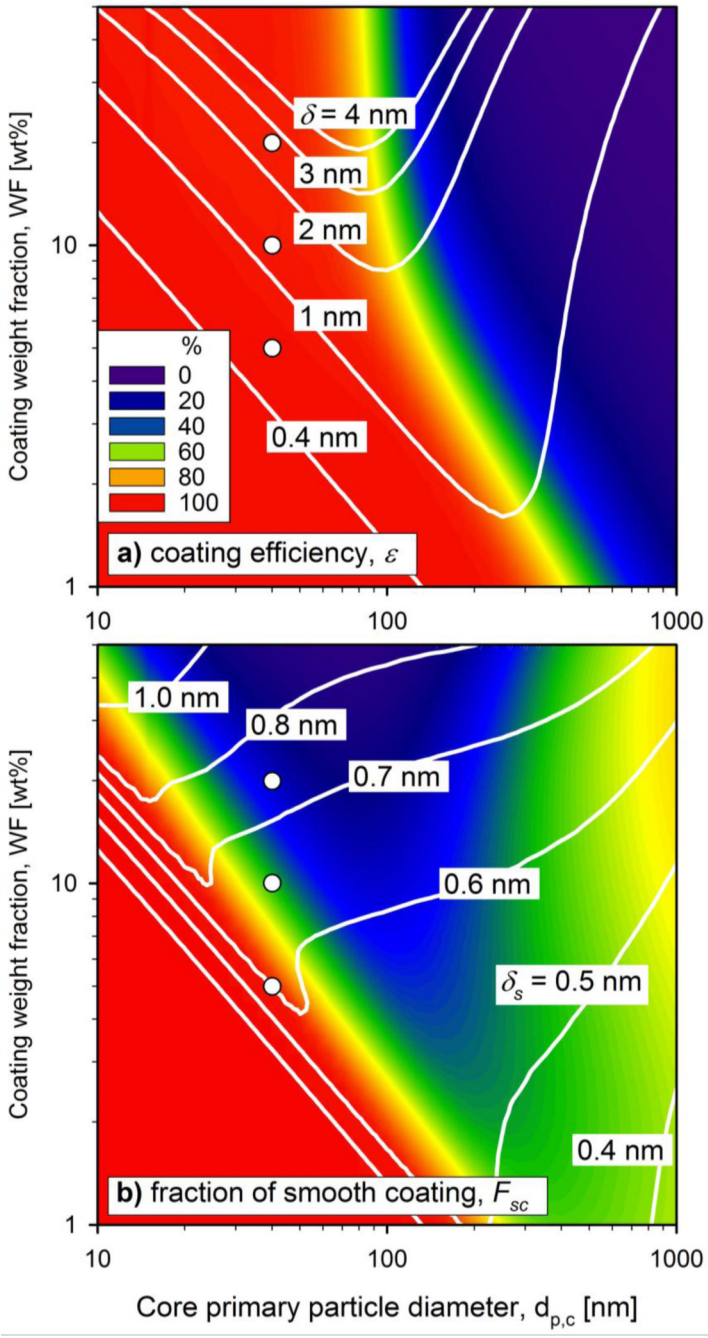

Figure 8.

The influence of core primary particle diameter and coating weight fraction on a) coating efficiency and b) fraction of smooth coating at the outlet of the coating unit (t = 0.1 s). The white contour lines correspond to a) total and b) smooth coating thickness. The white circles correspond to the data of Teleki *et al.* (2008a).